Advances in Science and Technology Research Journal

Advances in Science and Technology Research Journal, 2026, 20(9), 244–258
https://doi.org/10.12913/22998624/222456
ISSN 2299-8624, License CC-BY 4.0

Received: 2026.05.05
Accepted: 2026.07.12
Published: 2026.08.01

Numerical investigation of crack initiation and propagation in rock with installation clearances in undercut anchor systems

Józef Jonak[1], Robert Karpiński[1*]

[1] Department of Machine Design and Mechatronics, Faculty of Mechanical Engineering, Lublin University of Technology, Nadbystrzycka 36, 20-618 Lublin, Poland
* Corresponding author's e-mail: r.karpinski@pollub.pl

ABSTRACT

This study presents a numerical analysis of the initiation and propagation of cracks in a rock mass, accounting for installation clearances in the undercut anchor–borehole system. This is important for the context of rock de-consolidation technology and the assessment of the load-bearing capacity and performance of undercut anchors, where actual installation conditions deviate from ideal assumptions. In particular, the limitations of classical failure cone models are highlighted, as they do not reflect the actual trajectory of fracture propagation in brittle media. The aim of this study was to determine the influence of geometric clearances (l_1, l_2) between the anchor and the rock mass on the location of the fracture initiation point and the course of its propagation. The analysis was performed using the finite element method with the XFEM implemented in ABAQUS. Five clearance combinations in the range of 0–1 mm were considered, with a constant effective anchorage depth (h_{ef} = 70 mm) and unchanging material and geometric parameters of the system. The results indicate that, within the analyzed range of clearance values, their effect on the crack-propagation trajectory is negligible, and the crack paths are similar. However, it was found that, in selected configurations, the location of the crack initiation point may change, due to local stress redistribution in the contact zone, particularly near the drive screw tip. These results confirm that factors such as the rock's mechanical properties, the anchor head's geometry, and contact conditions are more significant in forming the failure zone than minor potential installation clearances. The conducted research makes a significant contribution to the development of methods for analyzing the performance of rock bolts in rock masses, indicating the limited significance of geometric imperfections within the analyzed scope and emphasizing the need for further research that accounts for more complex operating conditions of the system.

Keywords: undercut anchor, rock mechanics, crack propagation, XFEM, finite element analysis, failure zone, fracture mechanics, clearance effect.

INTRODUCTION

Anchors are structural components used in engineering structures in the broadest sense, serving as load-bearing connectors between structural elements and the ground or load-bearing medium [1–3]. They are used both in building and infrastructure construction (e.g., in securing steel structures to reinforced concrete elements) and in geotechnical and mining engineering, where they are employed for anchoring support structures, stabilizing rock mass, or carrying out rock mass detachment processes [4–6]. A special group consists of shear anchors, which, thanks to the specific geometry of the head and the mechanism of interaction with the substrate, enable the effective transfer of pull-out loads and the initiation of controlled failure processes in brittle materials. The complexity of anchor operating conditions stems from the interaction of numerous factors, including the mechanical properties of the rock mass, anchor geometry, contact conditions, and installation parameters, which means that their design and analysis must account for both material aspects and fracture mechanics [7–9]. Consequently, anchors play a significant role not only as structural elements but also as engineering tools used in modern technologies for the installation and excavation of rock masses [10–12].

Given the wide range of applications for undercut anchors, including the installation of steel structures in reinforced concrete buildings, the anchoring of offshore platforms, and the detachment of rock masses in one of the proposed disintegration technologies, researchers are primarily interested in the development of the anchor pull-out force - F (anchor load-bearing capacity) [13–16], depending on the effective anchorage depth h_{ef} and the mechanical properties of the medium (compressive strength) in which the anchor is embedded [17–21]. The general principle of anchoring using the ANZEX undercut bolt system is shown in Figure 1a, which illustrates the installation concept and load-transfer mechanism between the anchor and the surrounding medium [22]. The concept of the undercutting anchor's interaction with the rock and the CCD (Concrete Capacity Design) method's cone of destruction model [23] is illustrated in Figure 1b.

The analyses presented in [17,18] show that the maximum anchor pull-out force occurs at ~0.45 h_{ef} (point A, Figure 2, based on [24,25]), measured from the point where material cracking begins at the base of the anchor head. The formation of the failure zone in this case is not examined in detail (a simplified failure zone model in the form of a Conical Failure Surface or Four-sided Pyramid Failure Surface [26–28] is used - the dashed line in Figure 1b. As demonstrated by more extensive studies [24,29], in the case of brittle media (such as rock), the formation of the failure zone under the action of under-cutting anchors is a rather complex process that depends largely on the current combination of mechanical parameters of the tested medium [29–31] and significantly influences the extent of the failure zone, particularly the volume of the potentially created failure zone (the detached volume). Another group of factors determining the potential volume of the medium to be detached is the geometric parameters of the anchor head itself (e.g., the head angle β, [32–34]). From the perspective of the proposed technology for detaching rock masses by pulling out anchors, this aspect is particularly important (for determining the detachment efficiency and the energy consumption of the process).

Studies [24,29] have shown that the crack path, as well as the shape and extent of the damage zone, differ significantly from the model case assumed in the CCD method [23], described by the cone angle a_{CCD} (Figure 2). For high-strength concretes, the actual crack path covers a larger area (described by curve 1, Figure 2) than that resulting from the model. For dense rocks, an approximately parabolic shape of the damage zone is observed (curve 2, Figure 2). In contrast, for weak gray sandstone-type rocks, the shape of the damage zone is very complex. Initially, the fracture penetrates into the material along a paraboloid (curve 3, Figure 2) up to the inflection point B, and then follows a hyperbola toward the free surface. Point A defines a location on the fracture trajectory used in the CCD method to determine the theoretical angle of the cone of failure a_{CCD}, at which the maximum anchor pull-out force F occurs. Points C and D illustrate locations on the free surface of the rock medium where the crack reaches the surface of the medium. Angles a_0 describe the direction of crack propagation in the

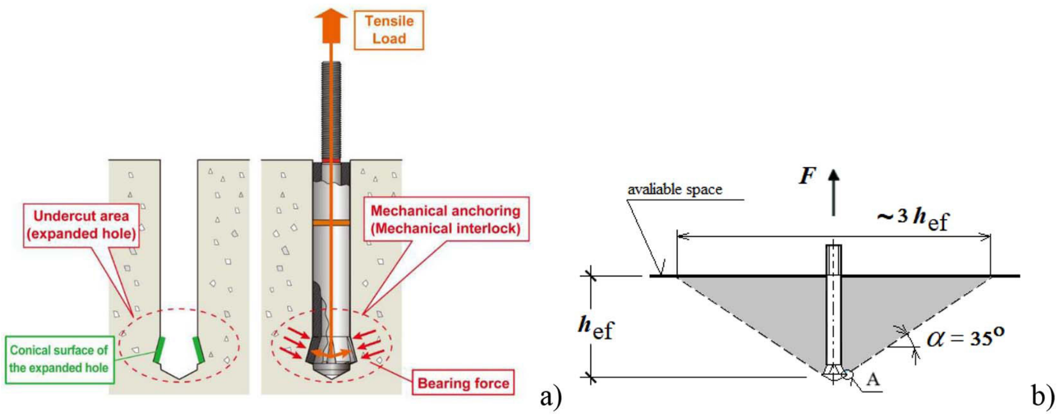

Figure 1. a) Principles of anchoring of an ANZEX bolt [22], b) simplified model (CCD method) of the failure zone in the medium under the action of an undercutting anchor: A - location of the crack initiation point

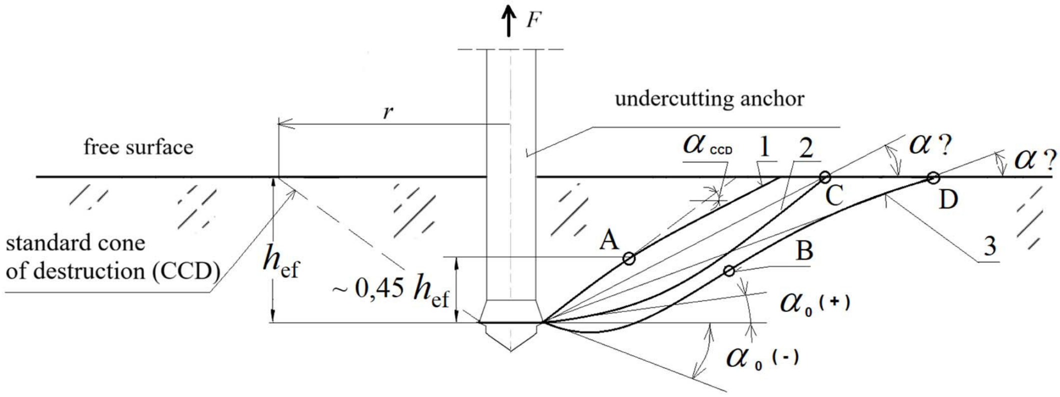

Figure 2. Fracture trajectory for various brittle materials: 1 – high-strength concrete, 2 – very high-strength rock, 3 – very brittle, gray sedimentary sandstone, h_{ef} – effective anchorage depth

initial phase of development, depending on the type of rock mass. Due to the complex shape of the fracture trajectory observed in practice, there is some discrepancy in estimating the angle of the failure zone*a*, which would be equivalent to that determined by the CCD method (a_{CCD}). Therefore, for field studies, as shown in Figure 2, points C and D were used as reference points in the procedure for estimating the geometric parameters of the damage zone, which differs significantly from the classic cone.

The original version of the rock de-bonding technology involved the pull-out of undercut anchors (e.g., the Hilti HDA-P) [35] using dedicated equipment; however, the size and weight of this machinery significantly limited the practical applicability of the method.

Subsequent studies [36] demonstrated the possibility of changing the load transfer method from the original approach, which involved pulling out the anchor embedded in the rock along with a separated cone-shaped block, to detaching blocks by fracturing the rock near the bottom of the hole, using a modified anchor design [29], as illustrated in Figure 3 [32].

In the solution shown in Figure 3, the anchor is installed with a certain clearance in a pre-drilled borehole in the rock mass. The borehole diameter corresponds to the size of the anchor head. In the initial stage, the rock is undercut by element 4-a conical undercutting head. The rotation of this element along the threaded drive screw 1, using a dedicated drive (not shown in the figure), results in its simultaneous axial movement and radial expansion of the undercutting elements over the conical nut 3. Consequently, the rock is undercut, forming a conical cavity that replicates the geometry of element 4. This operation also ensures the anchorage and expansion of the head within the undercut region.

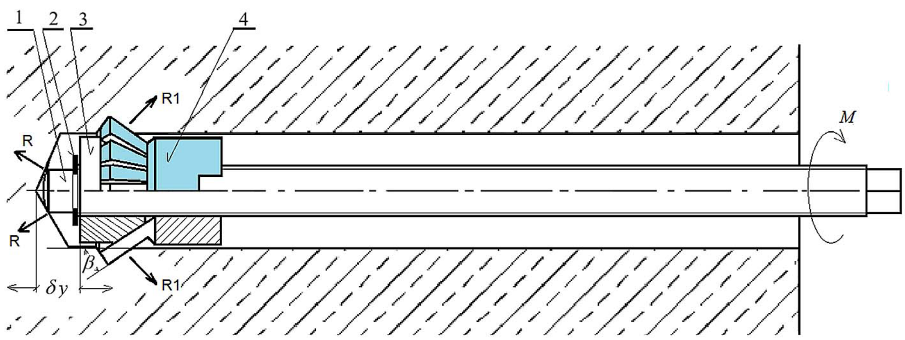

Figure 3. Cutting and loosening anchor: 1 – end of the anchor drive screw resting against the bottom of the rock borehole, 2 – retaining ring, 3, 4 – components of the conical anchor head (3 – conical nut, 4 – expansion ring), M – driving torque applied to the anchor's drive screw, *d*y – increment of relative displacement of the screw end and the conical anchor head, *R* – reaction forces at the contact between the screw end and the rock at the bottom of the hole, R_1 – reaction forces at the contact between the conical head element and the rock, *β* – angle of the conical head [32]

In the subsequent stage, torque is transmitted to screw 1, and the rotational motion of the drive screw is converted into linear displacement of the head along the screw axis. As the drive screw rotates, the head moves simultaneously toward the free surface of the rock mass (the distance δy between the bottom of the borehole and the undercutting head increases, as illustrated in Figure 4b). This process induces stress concentration at the base of the cutter head, leading to crack initiation and its progressive propagation, ultimately resulting in the formation of a so-called failure cone within the rock mass.

A number of studies conducted to date [29] have shown that the problem of damage zone propagation (in the form of a damage cone), particularly the formation of the potential detached volume, is complex [37]. The fracture trajectory is influenced by several factors [19,24,38]:

- mechanical properties of the rock mass (Young's modulus, compressive strength f_c, Poisson's ratio n, coefficient of friction between the rock and the steel head μ,
- geometric parameters of the bit (angle of the bit cone β – after expansion, length of the bit cone generatrix),
- actual combination of geometric parameters of the bit and the undercut hole), as illustrated in Figure 4a.

Dimensions l_1 and l_2 in Figure 4 represent the clearances between the anchor surface and the borehole surface. Dimensions b and e, on the other hand, characterize the position of the lower edge of the undercutting head, while angle l is the angle of the borehole bottom (which depends on the drilling technology used). All these dimensions, in the context of fracture mechanics, may be significant due to the shape and dimensions of the undercut in the rock (treated as a potential notch with specific geometric characteristics) and the direction of the applied load. The influence of the angle l has been indirectly investigated and described in studies [13,24], where its significance (along with the geometry of the drive screw tip) in determining the location of the initiation point of crack propagation accompanying the formation of the so-called cone of destruction was established.

Based on the presented review of the current state of knowledge and the results of previous studies, it can be concluded that the problem of crack propagation and the formation of a failure zone in brittle media under the action of undercut anchors is a complex and multi-parameter issue. Previous approaches have mainly focused on the influence of rock-mass mechanical parameters and the geometry of the anchor head, although analyses often employ simplified fracture-zone models (e.g., the CCD conical model) that do not reflect the actual fracture trajectories observed in rocks. At the same time, it is noted that the actual geometry of the failure zone may differ significantly from theoretical models, taking parabolic or more complex forms (as shown in Figure 2).

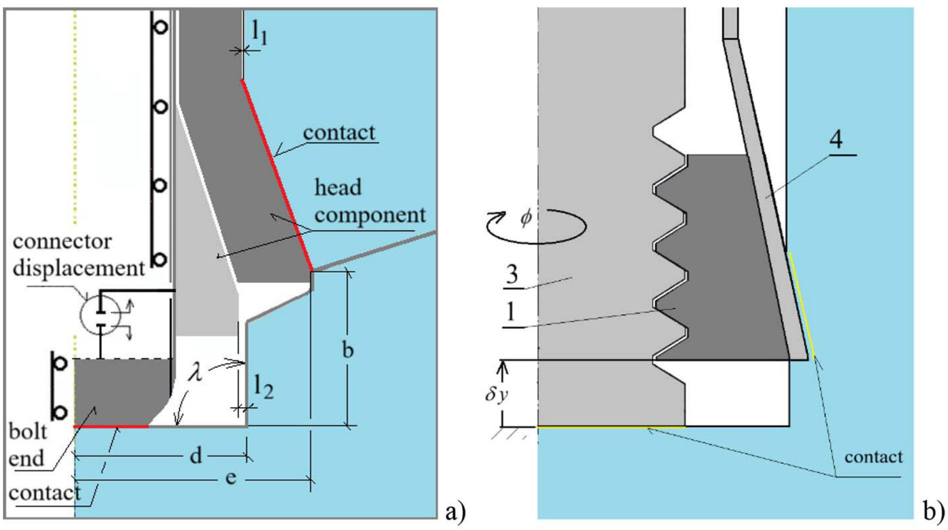

Figure 4. a) Rock model with a undercut, anchor drive screw, and head assembly
Note: Characteristic dimensions of the assembly: undercut head – drive screw – undercut hole, b) axial cross-section through the screw and undercut head components (designations as in Figure 3), *d*y – relative distance between the bottom of the hole and the head

In this context, there is a noticeable research gap regarding the influence of geometric imperfections in the anchor–hole system, particularly regarding installation clearances resulting from drilling and installation conditions [39,40]. The approach proposed in this paper introduces significant novelty through a systematic analysis of the influence of clearances l_1 and l_2 on the location of crack initiation and the progression of its propagation, using advanced XFEM numerical modeling. This allows for a more realistic representation of the anchor's operating conditions in rock and verification of the significance of parameters previously overlooked or treated as marginal.

The aim of this study was to numerically investigate the influence of installation clearances between the cut-in anchor and the rock mass (parameters l_1 and l_2) on the location of the fracture initiation point and the propagation path of cracks in brittle material. The analysis was conducted using the finite element method, with the XFEM algorithm implemented, to determine the significance of installation clearances on the formation of the failure zone and the potential volume of dislodged rock.

MATERIALS AND METHODS

Given the uncertainties identified to date regarding the influence of the geometric parameters described above (Figure 4) at the interface between the undercut anchor and the rock mass, this study attempts to clarify the effect of the clearance values between the rock and the anchor (l_1 and l_2, Figure 4) on the location of the initiation point and the propagation of rock fracturing under the action of the anchor structure in question. Ultimately, this translates to the potential volume of rock matrix that can be detached. The values of these parameters may be influenced by technological factors such as: the accuracy of the borehole (diameter), the correct selection of the drill bit diameter for the anchor borehole, the condition of the tool, etc. The combinations of the clearances under consideration were used for the analysis (Table 1).

Table 1. Combinations of installation clearances (l_1, l_2) considered in the numerical analysis of the anchor–rock system

Clearance combination ID	Clearance l_1(mm)	Clearance l_2(mm)
a	0	0
b	0.5	0
c	0.5	0.5
d	0.5	1
e	1	1

The remaining geometric parameters, including the anchorage depth h_{ef} = 70 mm = const., and the nominal geometric dimensions of the anchor = const. (including d = 22.5 mm, e = 28.15 mm, b = 17.9 mm, as shown in Figure 5), the physical and mechanical parameters of the matrix as well as the contact zone between the anchor and the matrix were not altered.

In case (a), i.e., when $l_1 = l_2 = 0$ mm, the dimensions of the hole above and below the head correspond to the nominal dimensions of the anchor hole – there is no clearance to consider.

The model dimensions were selected based on the effective anchoring depth to avoid potential stress influences from the model edge fixings and to allow the crack to propagate freely to the free surface of the medium. For an anchoring depth of 70 mm, the length of the model's horizontal side was set to 500 mm and the length of the model's vertical side to 300 mm.

Material properties

The rock mass was treated as a linear, elastic, isotropic material with the following parameters: Young's modulus – 14,275 MPa, Poisson's ratio – 0.247. The simulation was performed using ABAQUS v.2022 [41], together with the XFEM algorithm [42]. The brittle fracture condition was applied, which implies that the failure path is determined by the maximum tensile stress. The direction of propagation is defined as perpendicular to the direction of the maximum tensile stresses. The development of failure is determined by the fracture energy. Therefore, the following was specified in the program (according to ABAQUS procedures): Failure model – "Max Principal Stres.". The failure (tensile) stress was set to f_t = 7.74 MPa, and the Fracture Energy was set to 0.17 N/m, using a linear model. Stabilization factor 1E-06.

The steel from which the anchor components are made was also treated as a linear, elastic, and isotropic material (operating in the elastic range). Young's modulus 210,000 MPa, Poisson's ratio 0.3.

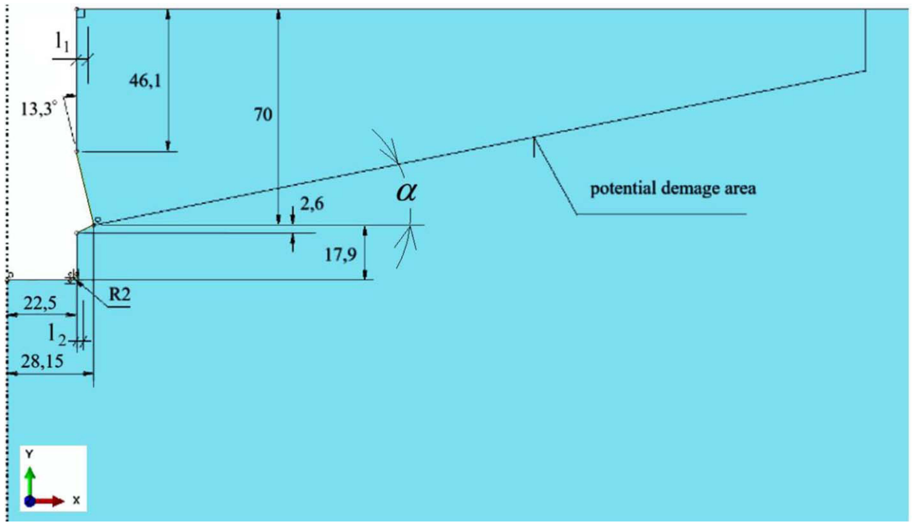

Figure 5. Geometric dimensions of an axially symmetric rock mass model with a cutout for an anchor in the spread position: l_1, l_2 – dimensions (clearances) subject to change during modeling; α – hypothetical angle of the failure surface (estimated experimentally)

Model specifications

Treating the model in Figure 5 as axially symmetric, the model nodes were fixed as shown in Figure 6. For the nodes on the right edge of the model, only the Y-axis displacement was allowed. For the bottom edge, displacement was allowed only along the X-axis. Due to the symmetry condition, the left edge of the model (along the screw axis) allows linear displacement only along the Y-axis. Similarly, for the connector nodes, only linear displacement along the Y-axis is permitted.

The model assumes contact between the rock mass and the components of the drive screw only in the area where the screw face contacts the bottom of the borehole and on the conical portion of the anchor head, as shown in Figure 6b. Using the ABAQUS software options, a "Penalty contact" type was applied with a contact friction coefficient of $\mu = 0.2$. To implement the kinematic constraint, "Connector displacement" finite elements available in ABAQUS were used. Such a connector has two nodes (A, B, Figure 6b), the distance between which can be changed programmatically in discrete steps by controlling the relative position of the drive screw and the cutting head. Node A of the connector was connected to three nodes of the undercutting head assembly via three rigid tie elements, treated as a monolith. In turn, node B of the connector is connected to the three end nodes of the screw. This solution allows for a controlled change in the position of the head relative to the end of the screw by changing the distance between the connector nodes (d, Figure 6b). The parameter

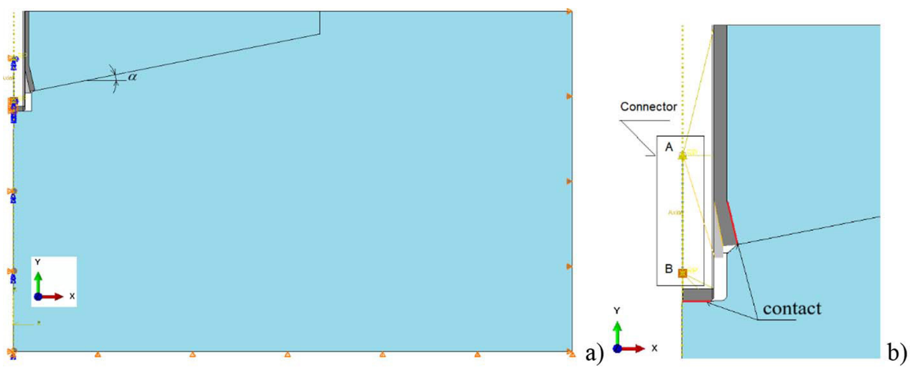

Figure 6. a) Model node constraints, b) method of applying kinematic constraints using ABAQUS "Connector" elements, α – angle of the hypothetical fracture surface

d was varied iteratively, with an increment of 0.01 mm in each step, up to a maximum value of 10 mm, while maintaining the convergence condition of the calculations (algorithm pause) by observing the propagation of the gap during the simulation.

Finite element mesh

To verify the sensitivity of the model to mesh geometric parameters, different finite element meshes were employed during the analyses (Figure 7). The primary difference concerned the orientation of the assumed crack initiation surface, defined either at an angle of α = 20° (as adopted in previous numerical analyses validated by experimental studies, e.g., [25,27]) or at α = 0° (Figure 7b).

The mesh was constructed using axisymmetric stress elements with linear shape functions and reduced integration, specifically 4-node elements of type CAX4R.

For the rock mass model, a global mesh size of 25 mm was used; in the area of contact with the anchor, 2 mm; in the area of contact with the bolt, from 0.9 to 1.52 mm; a transition radius at the bottom of the hole of 2 mm; at the edge in the upper part of the solid, the mesh size varied from 3 to 10 mm; and along the line of the predicted fracture, it ranged from 5 to 10 mm. The number of nodes was approximately 1.541, and the number of elements was approximately 1.458.

For the anchor, linear quadrilateral CAX4R elements and linear triangular CAX3 elements were used. For the bolt, linear quadrilateral elements of type CAX4R and linear triangular elements of type CAX3 were used.

Studies conducted to date have shown that the geometric parameters of the mesh elements have a negligible effect on the resulting fracture trajectories (low sensitivity of the geometric model of the medium to the finite element mesh parameters), which also confirms the robustness of the XFEM algorithm used with respect to the finite element mesh geometry, as noted in the literature on the subject [43] and demonstrated in the authors' studies [29].

RESULTS

The results of the analyses are presented in Figure 8, where Figures a, c, e, g, and i show the distribution of normal maximum stresses σ_{max} within the penetrating crack for the clearance combinations listed in Table 1, while Figures b, d, f, h, and j illustrate the formation of the initiation site and the fracture trajectory for the considered clearance combinations.

For improved visualization of the results, all crack propagation trajectories obtained in the analysis are collectively presented in Figure 9.

The results indicate that, for the assumed anchorage depth, crack initiation points are generally located within the region of the rounding radius R of the anchor borehole model. Only in the case of clearance combination b (l_1 and l_2), the initiation point is shifted directly beneath the end of the drive screw and slightly below the surface of the medium. This corresponds to the crack initiation location observed in a typical Hertzian contact problem (as previously reported in [13], where it was shown that for undercut anchors expanded near the bottom of the borehole, the crack initiation

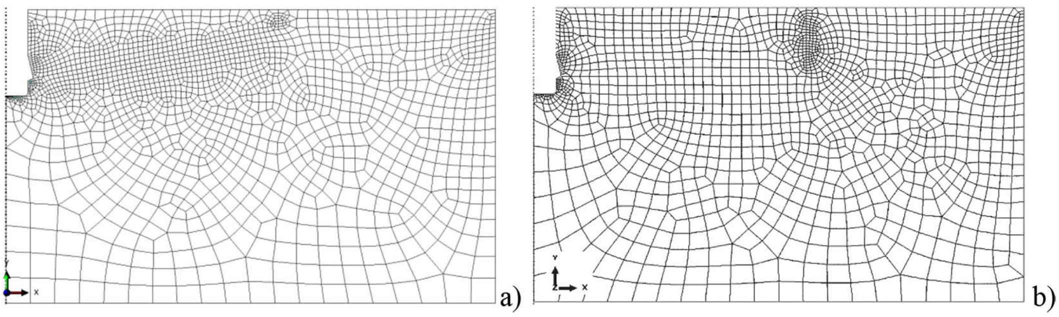

Figure 7. Finite element mesh configurations used in the numerical analysis of the anchor–rock system: (a) mesh with the assumed initial crack orientation at an angle of α = 20°, consistent with previous numerical studies validated experimentally; (b) alternative mesh configuration with the crack initiation surface oriented at α = 0°

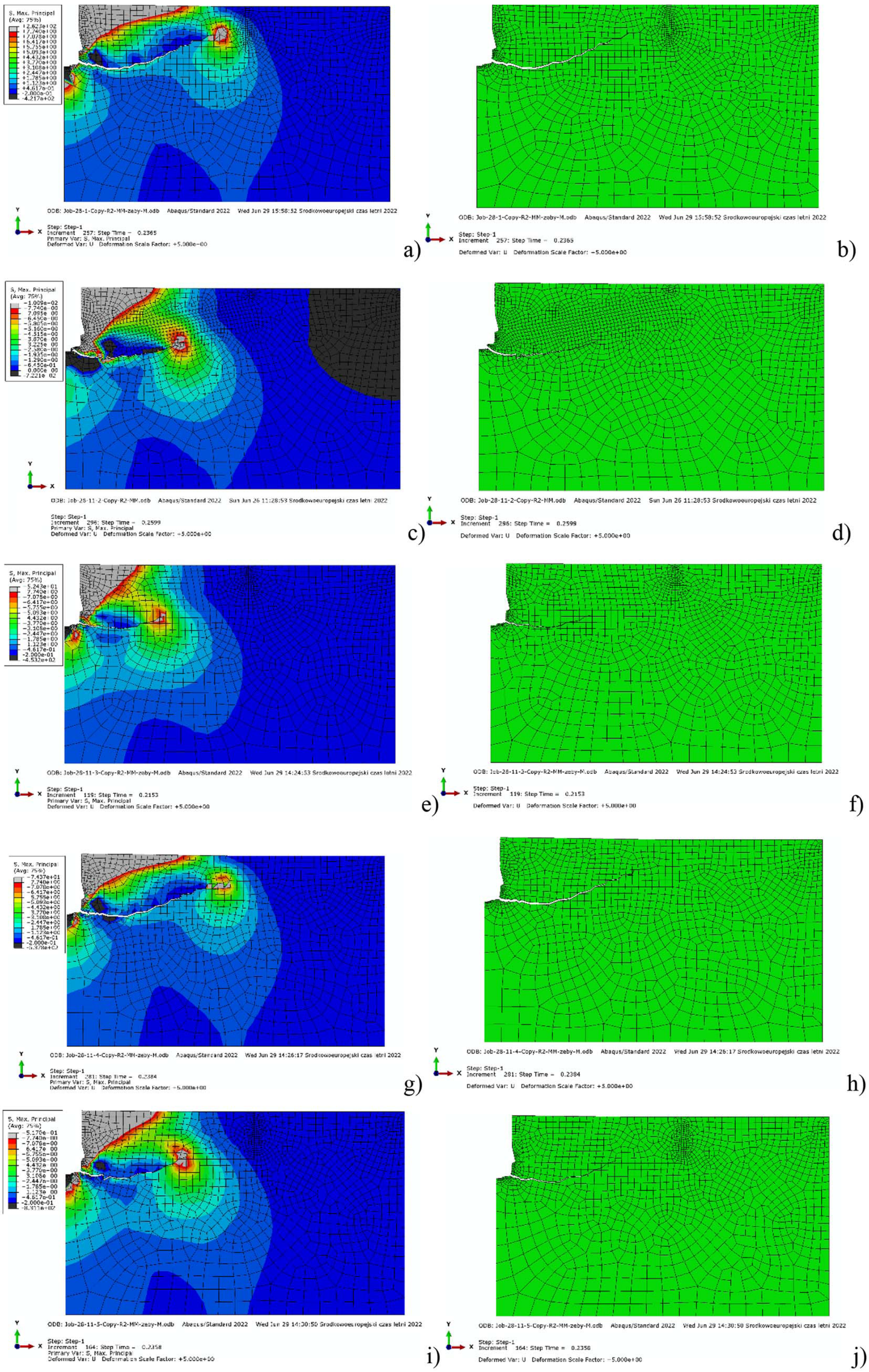

Figure 8. (a, c, e, g) – distribution of maximum principal normal stresses (σ_{max}); (b, d, f, h, j) – crack initiation locations and crack propagation paths for the considered clearance combinations, respectively, according to Table 1.

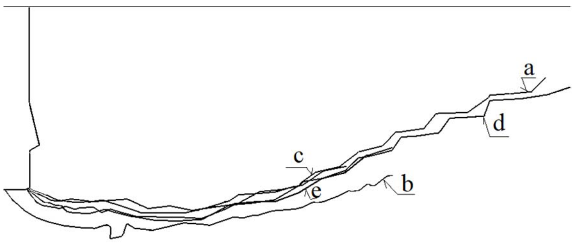

Figure 9. Crack initiation points and crack propagation trajectories obtained for the considered clearance combinations
Note: Individual combinations are denoted by letters in accordance with Table 1.

point is located in the contact zone between the drive screw tip and the borehole bottom, rather than at the base of the undercutting head). This aspect requires further detailed investigation in a separate study.

It can also be observed that the crack trajectories largely overlap or locally intersect, indicating that the considered clearances do not significantly influence the formation and development of crack propagation paths.

The obtained results are also consistent with the authors' previous studies on the effect of borehole diameter (with other parameters held constant) on the crack trajectory [44], where it was demonstrated that the borehole diameter (and thus the corresponding anchor diameter) does not significantly affect the course or extent of crack propagation.

DISCUSSION

The aim of this study was to investigate whether geometric clearances between the cut-in anchor and the installation hole (l_1, l_2 in the range of 0–1 mm) affect the location of crack initiation and the subsequent fracture path in gray sandstone. An axisymmetric FEM/XFEM model in ABAQUS [45] was used, with a constant effective anchorage depth h_{ef} = 70 mm, to analyze five combinations of l_1/l_2. This methodological setup effectively isolates a single geometric problem and allows for the assessment of whether minor installation deviations can control the crack path in a brittle medium.

Numerical studies constitute an invaluable complement to experimental investigations. They enable a substantial reduction in design time and costs by allowing virtual testing of structural variants without the need for expensive prototypes [46–49]. They enable extensive parametric analysis and optimization (e.g., sensitivity analysis of model parameters) and the simulation of extreme operating conditions. This contributes to a deeper understanding of complex phenomena and enhances structural safety [50]. Despite these advantages, numerical methods have inherent limitations (e.g., simplified models and approximations) and must always be experimentally validated to ensure the reliability of the results [51,52].

The most important finding is of an ordering nature: within the analyzed range of clearances, the crack propagation trajectories remain very similar, suggesting that the individual parameters l_1 and l_2 are not primary factors governing the shape of the failure zone [53]. At the same time, a notable exception is observed for the case l_1 = 0.5 mm and l_2 = 0 mm, in which the crack initiation point shifts toward the end of the drive screw. This result does not exclude the influence of clearances per se, but rather indicates that their role may be secondary to local stress redistribution in the contact zone and the geometry of load transfer. Such an interpretation is consistent with recent studies showing that factors such as the rock's mechanical properties, friction at the contact zone, and the anchor head's geometry exert a stronger influence than minor dimensional variations.

Although the present study was primarily focused on crack initiation and propagation rather than on the detailed mechanical response of the anchor itself, the numerical results allow several general observations regarding strain distribution and displacement behavior to be formulated. The deformation of the anchor–rock system is governed mainly by the local contact interaction between the conical anchor head, the drive screw tip, and the surrounding rock mass. The highest stress and strain concentrations are expected in the immediate vicinity of these contact zones, particularly near the borehole bottom and the rounded region of the undercut. Within the analyzed clearance range, no substantial change in the global displacement pattern of the anchor system was observed; however, local changes in contact conditions may shift the crack initiation point, as demonstrated for the l_1 = 0.5 mm and l_2 = 0 mm configuration. This indicates that the rock bolt's displacement behavior remains largely controlled by the anchor-head geometry and the local load-transfer mechanism. In contrast, minor installation clearances mainly affect local stress redistribution rather than the overall deformation mode. Therefore, no fully generalized conclusion on strain distribution in the anchor can be drawn at this stage, and this aspect should be examined in future studies using extended 3D models and experimental force–displacement validation.

The position of the fracture initiation point and the subsequent crack propagation pattern are directly related to the mechanism by which the anchor transfers load to the surrounding rock mass. In the classical pull-out mechanism, a deeper and more inward-oriented fracture trajectory may be associated with a larger potentially detached rock volume and, consequently, with higher anchor load-bearing capacity. This is consistent with previous observations indicating that fracture paths penetrating deeper into the rock mass, particularly those corresponding to smaller equivalent cone angles, generally require higher pull-out forces. However, in the present study, force measurements were performed only for anchors subjected to pull-out loading. For the anchor configuration in which failure initiates near the borehole bottom due to interaction between the drive screw tip and the rock, direct measurement of the destructive force was not possible because of current experimental and technological limitations. Therefore, the relationship between the numerically identified initiation point, the failure-zone geometry, and the actual load-bearing capacity should be interpreted qualitatively rather than quantitatively.

The numerical results indicate that the analyzed clearances do not significantly alter the overall propagation pattern of the failure zone, suggesting that minor installation clearances within the investigated range are unlikely to affect the anchor's global load-bearing response substantially. Nevertheless, the local shift of the crack initiation point observed for the $l_1 = 0.5$ mm and $l_2 = 0$ mm configuration indicates that stress redistribution in the contact zone, especially near the drive screw tip and the borehole bottom, may influence the initial stage of failure. The failure zones identified in the numerical model should therefore be interpreted as regions of localized tensile stress concentration and progressive loss of rock continuity, which determine the direction of crack development and the potential detached volume. In practical terms, this confirms that the load-bearing capacity of the anchor is controlled not only by the nominal anchorage depth, but also by the geometry of the anchor head, the ratio between the undercut/head diameter and the borehole diameter, the local contact conditions, and the possible plasticization or crushing of the rock in the contact ring. Further experimental work, including direct measurement of the force at the contact between the screw tip and the borehole bottom, is necessary to quantitatively link the numerically predicted failure zones with the destructive force and the anchor's actual load-bearing capacity.

Against the background of the literature from 2021 to 2025, the obtained results are largely consistent. Jonak et al. [19] demonstrated that the physico-mechanical properties of the rock and friction in the contact zone significantly influence the extent of the initial failure zone. At the same time, studies focused on the anchor head angle have shown that head geometry strongly governs both the extent of detachment and the direction of crack propagation.

In turn, investigations of gray sandstone on anchor diameter and h_{ef} revealed no clear, monotonic relationship for the initial crack angle or trajectory, supporting the conclusion that l_1 and l_2 should be considered secondary rather than dominant parameters. At the same time, studies of the drive screw tip geometry and the borehole bottom have shown that local contact geometry can shift the crack initiation point toward the screw region – precisely as observed for the case $l_1 = 0.5$ mm and $l_2 = 0$ mm.

From a practical perspective, the study reinforces the view that, in planning and optimizing rock detachment technologies, greater priority should be given to the mechanical properties of the rock, the geometry of the anchor head and drive screw tip, and the borehole bottom geometry, rather than to minor installation clearances. At the same time, the lack of experimental validation does not yet allow this conclusion to be considered definitive.

The adopted rock-mass model should therefore be interpreted as an idealized representation of intact sandstone specimens rather than a direct representation of a naturally fractured rock mass. Assuming a continuous, homogeneous, and isotropic medium provides an upper-bound estimate of the anchor pull-out resistance, because the presence of natural discontinuities, joints, bedding planes, or pre-existing microcracks would generally reduce the medium's effective stiffness, tensile resistance, and fracture energy. Consequently, fractures in the rock mass may facilitate earlier crack initiation and reduce the pull-out force required to detach the rock volume. However, the influence of such discontinuities on the extent and shape of the detached zone is more complex. The orientation of bedding or fracture planes may either limit the failure zone locally or promote long-range crack propagation along preferential weakness planes, leading to highly variable and difficult-to-predict fracture trajectories. For this reason, the present results should be regarded as a reference case for intact sandstone. At the same time, future analyses should include weakened, anisotropic, stratified, and naturally fractured rock-mass models to evaluate the sensitivity of crack initiation, propagation path, pull-out force, and detached volume to realistic geological discontinuities.

The most justified directions for further research include:

- validation of the model through field or laboratory experiments, including the recording of force–displacement curves and the actual detached volume;
- development of 3D models incorporating torsional friction and mixed-mode fracture (I/II/III);
- extension of the analysis to anisotropic, fractured, and stratified rock media;
- combined analysis of l_1/l_2, β, drive screw tip and borehole bottom geometry, and material parameters, with rigorous calibration of fracture energy (G_f).

LIMITATIONS OF THE STUDY AND DIRECTIONS FOR FUTURE WORK

The presented results should be interpreted with consideration of the limitations arising from the adopted modeling assumptions and the scope of the analysis. The study was conducted for a single, constant value of the effective anchorage depth (h_{ef} = 70 mm), limiting the generalizability of the results to other geometric configurations of the anchor–rock system. Variations in anchorage depth affect the stress distribution and equilibrium conditions in the model, potentially leading to different locations of crack initiation and propagation paths.

The assumption of a linear-elastic, isotropic material model for the rock mass constitutes an additional simplification, as real rocks often exhibit nonlinear behavior, anisotropy, and structural discontinuities, all of which may significantly alter the failure mechanism [54].

Additionally, the use of an axisymmetric numerical model does not allow for the representation of three-dimensional spatial effects, such as asymmetric crack propagation or local stress concentrations resulting from installation imperfections [55]. Another important limitation is the assumption of constant contact parameters, including the coefficient of friction, without accounting for their variability under different operating conditions.

Furthermore, the scope of the analysis was limited to relatively small installation clearances (l_1, l_2 in the range 0–1 mm), corresponding to typical technological tolerances, but did not cover extreme cases, execution errors, or the effects of drill bit wear.

Moreover, the interaction between installation clearances and other important geometric and material parameters, such as the anchor head angle, the geometry of the drive screw tip, and rock mass properties, was not analyzed, even though these factors may exert a dominant influence on crack initiation and propagation. The simplified approach to fracture modeling, based on the maximum principal stress criterion and a prescribed fracture energy, does not fully capture the complex failure mechanisms occurring in brittle materials.

The obtained results indicate the need to extend the research in several key directions. First and foremost, experimental validation of the model is required under both laboratory and field conditions, including the measurement of force–displacement relationships and the observation of the actual geometry of the failure zone. This would enable an assessment of the consistency between numerical predictions and the rock mass's actual behavior, as well as the identification of potential discrepancies arising from the adopted modeling simplifications.

The next step should involve developing numerical models for full three-dimensional (3D) analyses that incorporate complex contact conditions and mixed-mode fracture (I/II/III) [55]. Particular emphasis should be placed on accurately representing the real geometry of the anchor–borehole system, including installation imperfections and load asymmetry.

An important direction for future research is to extend the analysis to various rock media, including anisotropic, fractured, and layered materials, to assess the influence of internal structure on crack initiation and propagation mechanisms. At the same time, a comprehensive multi-parameter analysis is recommended that accounts for the combined effects of installation clearances, anchor head geometry, contact parameters, and rock mechanical properties.

Additionally, future studies should account for the influence of fracture energy parameters (e.g., fracture energy G_f) and their calibration based on experimental data. This would enable a more accurate representation of the failure process and improve the predictive capability of numerical models.

In the longer term, it will also be important to link numerical results to the optimization of rock detachment technologies, particularly in terms of process energy efficiency and the maximization of the controlled detached volume [56].

CONCLUSIONS

The conducted numerical analyses using the finite element method and the XFEM algorithm have shown that, within the considered range of installation clearances (l_1, l_2 = 0–1 mm), their influence on crack propagation trajectories in the rock mass is negligible, and the obtained crack paths remain very similar. At the same time, variations in clearance values may locally shift the crack initiation point, associated with stress redistribution in the contact zone, particularly near the drive screw tip.

The results indicate that geometric imperfections arising from the installation process are less important for crack initiation and propagation than factors such as rock mechanical properties, anchor head geometry, and contact conditions. This implies that, in the analysis and design of anchoring systems, greater emphasis should be placed on the rock mass's material parameters and the structural design of the anchor head rather than on manufacturing tolerances within the analyzed range.

The study also confirms the limited adequacy of simplified conical models (e.g., CCD) for describing the actual fracture behavior in brittle media, pointing to the more complex nature of the failure zone. At the same time, the results constitute a meaningful contribution to the modeling of undercut anchor performance. They may serve as a basis for further research that incorporates more complex operating conditions, including three-dimensional analyses and the experimental validation of numerical models.

REFERENCES

1. Chen Z. Non-concrete breakout failure modes of concrete mechanical anchors in tension-a literature review. Construction and Building Materials. 2023 Feb;366:130222. https://doi.org/10.1016/j.conbuildmat.2022.130222
2. Cao Y, Hua X, Zhang H. Influence of adjacent undercutting line positions on surrounding rock stability in block caving. Sci Rep. 2025 Nov 27;15(1):45454. https://doi.org/10.1038/s41598-025-28625-y
3. Manquehual CJ, Li CC, Shabanimashcool M, Grindheim B, Lia L. 3D numerical modeling of rock mass failure in an uplift test of a rock anchor with focus on the role of rock joints. Rock Mech Rock Eng. 2025 Mar;58(3):2847–75. https://doi.org/10.1007/s00603-024-04315-5
4. Camposinhos RS. Undercut anchorage in dimension stone cladding. Proceedings of the Institution of Civil Engineers - Construction Materials. 2013 Jun;166(3):158–74. 1.
5. Chen Z. Non-concrete breakout failure modes of concrete mechanical anchors in tension-a literature review. Construction and Building Materials. 2023 Feb;366:130222. https://doi.org/10.1016/j.conbuildmat.2022.130222
6. Cao Y, Hua X, Zhang H. Influence of adjacent undercutting line positions on surrounding rock stability in block caving. Sci Rep. 2025 Nov 27;15(1):45454. https://doi.org/10.1038/s41598-025-28625-y
7. Manquehual CJ, Li CC, Shabanimashcool M, Grindheim B, Lia L. 3D numerical modeling of rock mass failure in an uplift test of a rock anchor with focus on the role of rock joints. Rock Mech Rock Eng. 2025 Mar;58(3):2847–75. https://doi.org/10.1007/s00603-024-04315-5
8. Camposinhos RS. Undercut anchorage in dimension stone cladding. Proceedings of the Institution of Civil Engineers - Construction Materials. 2013 Jun;166(3):158–74. https://doi.org/10.1680/coma.11.00050
9. Sharma A, Mahadik V, and Hofmann J. Influence of tension loading protocol on crack cycling tests on undercut anchors. Structural Journal. 2016 Jul 1;113(4). https://doi.org/10.14359/51688622
10. Le Noir De Carlan M, Jason L, Davenne L. Numerical simulation of anchor pullout and shear

tests using a regularized damage model. Applied Sciences. 2024 Dec 3;14(23):11262. https://doi.org/10.3390/app142311262
11. Lu W, Luo K, Yan X, Li D, Ren R. Anchoring performance of a novel two-section pressure-tension composite anchor for earthen sites conservation. npj Herit Sci. 2025 Dec 3;13(1):627. https://doi.org/10.1038/s40494-025-02209-5
12. Olsen J, Pregartner T, Lamanna AJ. Basis for design of screw anchors in concrete. ACI Structural Journal. 2012;109(4).
13. Di Nunzio G, Muciaccia G. A combined concrete cone breakout—pull-out model for cast-in-place fasteners. Structural Concrete. 2025 Aug;26(4):4682–96. https://doi.org/10.1002/suco.202400926
14. Jeon S, Ju M, Park J, Choi H, Park K. Prediction of concrete anchor pull-out failure using cohesive zone modeling. Construction and Building Materials. 2023 Jun;383:130993. https://doi.org/10.1016/j.conbuildmat.2023.130993
15. Yang Z, Zhu W, Guan K, Yan B, Luo W, Liang P. Experimental and numerical study on the anchorage effect of bolted jointed rock masses. Front Earth Sci. 2022 Mar 17;10:861912. https://doi.org/10.3389/feart.2022.861912
16. Jiang Y, Li X, Liu J, Luan H, Zhang S, Wang C, et al. Study on shear behavior and failure characteristics of bolted anisotropic rock joints. Materials. 2023 Mar 9;16(6):2210. https://doi.org/10.3390/ma16062210
17. Jonak J, Karpiński R, Wójcik A. Parametric study of the effect of anchor drive bolt geometry on stress distribution and direction of crack formation in the rock medium. Materials. 2025 Sep 3;18(17):4136. https://doi.org/10.3390/ma18174136
18. ANZEX Undercut Anchor System Installation Manual. Installation Manual for ANZEX Undercut Anchor System [Internet]. ANZEX 714-00E / 617-00E. 2021 [cited 2026 Apr 28]. Available from: https://www.miyanaga.co.jp/engl/products/anzex/pdf/mi_ANZEX-D_manual.pdf
19. Aboayanah KR, Abdelaziz A, Haile BF, Zhao Q, Grasselli G. Evaluation of damage stress thresholds and mechanical properties of granite: New insights from digital image correlation and GB-FDEM. Rock Mech Rock Eng. 2024 Jul;57(7):4679–706. https://doi.org/10.1007/s00603-024-03789-7
20. Xue F, Lin Z, Wang T. Experimental study on cracking process and fracture properties of granite under mode I loading by acoustic emission and digital image correlation. Fatigue Fract Eng Mat Struct. 2023 May;46(5):1921–36. https://doi.org/10.1111/ffe.13973
21. Eligehausen R, Mallée R, Silva JF. Anchorage in concrete construction. Vol. 10. Wiley Online Library; 2006.
22. Eligehausen R, Sawade G. A fracture mechanics based description of the pull-out behavior of headed studs embedded in concrete [Internet]. Universität Stuttgart; 1989 [cited 2024 Dec 29]. Available from: http://elib.uni-stuttgart.de/handle/11682/7947. https://doi.org/10.18419/OPUS-7930
23. Jonak J, Karpiński R, Wójcik A, Siegmund M. The influence of the physical-mechanical parameters of rock on the extent of the initial failure zone under the action of an undercut anchor. Materials. 2021 Apr 8;14(8):1841. https://doi.org/10.3390/ma14081841
24. Eshraghi A, Rivard P, Moradian O, Kodjo SA, Shams G. Experimental investigation of cone-shaped failure mechanism in high-capacity post-tensioned anchors using ultrasonic active-passive monitoring. Construction and Building Materials. 2025 Feb;465:140251. https://doi.org/10.1016/j.conbuildmat.2025.140251
25. Sun DL, Rao Q hua, Wang SY, Yi W, Shen Q qing. A new mixed-mode fracture criterion of anisotropic rock. Engineering Fracture Mechanics. 2021 May;248:107730. https://doi.org/10.1016/j.engfracmech.2021.107730
26. Miyanaga Co. Ltd. Installation Manual for ANZEX Undercut Anchor System [Internet]. [cited 2026 May 21]. Available from: https://www.miyanaga.co.jp/engl/products/anzex/pdf/mi_ANZEX-D_manual.pdf
27. Fuchs W, Eligehausen R, Breen JE. Concrete capacity design (CCD) approach for fastening to concrete. Structural Journal. 1995;92(1):73–94.
28. Tomiczek K, Jonak J, Siegmund M, editors. Eksperymentalna i numeryczna analiza odspajania skał z użyciem kotew. Gliwice: Instytut Techniki Górniczej KOMAG; 2025. (Prace Naukowe, Monografie / KOMAG; no. 61). https://doi.org/10.32056/KOMAG/Monograph2025.7
29. Jonak J, Karpiński R, Wójcik A, Siegmund M. Numerical investigation of the formation of a failure cone during the pullout of an undercutting anchor. Materials. 2023 Feb 28;16(5):2010. https://doi.org/10.3390/ma16052010
30. Hariyadi, Munemoto S, Sonoda Y. Experimental analysis of anchor bolt in concrete under the pull-out loading. Procedia Engineering. 2017;171:926–33. https://doi.org/10.1016/j.proeng.2017.01.391
31. Jonak J, Karpiński R, Siegmund M, Machrowska A, Prostański D. Experimental verification of standard recommendations for estimating the load-carrying capacity of undercut anchors in rock material. Adv Sci Technol Res J. 2021 Mar 1;15(1):230–44. https://doi.org/10.12913/22998624/132279
32. Building code requirements for structural concrete (ACI 318-05) and commentary (ACI 318R-05). In. American Concrete Institute; 2005.

33. Jonak J, Karpiński R, Wójcik A, Siegmund M, Kalita M. Determining the effect of rock strength parameters on the breakout area utilizing the new design of the undercut/breakout anchor. Materials. 2022 Jan 23;15(3):851. https://doi.org/10.3390/ma15030851
34. Jonak J, Karpiński R, Wójcik A. Numerical analysis of the effect of embedment depth on the geometry of the cone failure. J Phys: Conf Ser. 2021 Dec 1;2130(1):012012. https://doi.org/10.1088/1742-6596/2130/1/012012
35. Jonak J, Karpiński R, Wójcik A. Numerical analysis of undercut anchor effect on rock. J Phys: Conf Ser. 2021 Dec 1;2130(1):012011. https://doi.org/10.1088/1742-6596/2130/1/012011
36. Wójcik A, Jonak J, Karpiński R, Jonak K, Prostański D, Kaczyński R. A numerical study of the influence of cone angle of the breakout anchor head on the crack trajectory of the medium. Adv Sci Technol Res J. 2024 Sep 1;18(5):101–12. https://doi.org/10.12913/22998624/190133
37. Jonak J, Karpiński R, Wójcik A. Influence of the undercut anchor head angle on the propagation of the failure zone of the rock medium. Materials. 2021 May 2;14(9):2371. https://doi.org/10.3390/ma14092371
38. Jonak J, Karpiński R, Wójcik A. Influence of the undercut anchor head angle on the propagation of the failure zone of the rock medium—Part II. Materials. 2021 Jul 12;14(14):3880. https://doi.org/10.3390/ma14143880
39. Hilti. Technical Datasheet Update: Dec-17, HDA UNDERCUT ANCHOR. [Internet]. Available from: https://www.hilti.co.uk/medias/sys_master/documents/he5/hff/9284064378910/Technical-data-sheet-for-the-HDA-design-anchor-Technical-information-ASSET-DOC-2331016.pdf
40. Wójcik A, Jonak K, Karpiński R, Jonak J, Kalita M, Prostański D. Mechanism of rock mass detachment using undercutting anchors: A numerical finite element method (FEM) analysis. Materials. 2024 Sep 11;17(18):4468. https://doi.org/10.3390/ma17184468
41. Mehraban MR, Bahrami B, Ayatollahi MR, Nejati M. A Non-local XFEM-based methodology for modeling mixed-mode fracturing of anisotropic rocks. Rock Mech Rock Eng. 2023 Feb;56(2):895–909. https://doi.org/10.1007/s00603-022-03134-w
42. Siegmund M, Jonak J. Analysis of the process of loosening the rocks with different strength properties using the undercutting bolts. IOP Conf Ser: Mater Sci Eng. 2019 Dec 1;679(1):012014. https://doi.org/10.1088/1757-899X/679/1/012014
43. Xue F, Tong Z, Chen W, Wang T, You X, Lin Z. Experimental study on anchorage mechanical effect of rock bolts on cross-jointed rock mass using DIC and AE. Theoretical and Applied Fracture Mechanics. 2025 Jun;137:104875. https://doi.org/10.1016/j.tafmec.2025.104875
44. Chen Y, Yu D, Wang Y, Zhao Y, Yang H, Huang L. Dynamic characteristics and anchorage mechanisms of fractured granite: analytical, numerical and experimental analyses. Rock Mech Rock Eng. 2025 Feb;58(2):1569–89. https://doi.org/10.1007/s00603-024-04249-y
45. Dassault Systèmes Simulia Corporation. Abaqus 2019. Velizy Villacoublay, France: Dassault Systèmes Simulia Corporation; 2019.
46. Xu B, Xu T, Xue Y, Heap MJ, Wasantha PLP, Li Z. Phase field modeling of mixed-mode crack in rocks incorporating heterogeneity and frictional damage. Engineering Fracture Mechanics. 2024 Mar;298:109936. https://doi.org/10.1016/j.engfracmech.2024.109936
47. Bazant ZP, Kazemi MT, Hasegawa T, Mazars J. Size effect in Brazilian split-cylinder tests. Measurements and fracture analysis. ACI Materials Journal. 1991;88(3):325–32.
48. Jonak J, Karpiński R, Wójcik A, Siegmund M. The effect of undercut anchor diameter on the rock failure cone area in pullout tests. Adv Sci Technol Res J. 2022 Nov 1;16(5):261–70. https://doi.org/10.12913/22998624/154894
49. Dabloul R, Jin BC, Jha B. Failure analysis of the edge-notched beam test on fluid-exposed Berea Sandstone. Acta Geotech. 2023 Aug;18(8):4035–53. https://doi.org/10.1007/s11440-023-01843-2
50. Kocaer O, Kul A. Parametric analysis of design and operational parameters in 3D concrete printing of wall elements. Journal of Building Engineering. 2025 Dec;115:114494. https://doi.org/10.1016/j.jobe.2025.114494
51. Ojeda-López A, Botana-Galvín M, González-Rovira L, Botana FJ. Numerical simulation as a tool for the study, development, and optimization of rolling processes: A review. Metals. 2024 Jun 21;14(7):737. https://doi.org/10.3390/met14070737
52. Karski S, Awtoniuk M, Szala M. Application of artificial intelligence methods to determine the optimal process parameters in resistance projection welding of steel nuts. Appl Comput Sci. 2026 Mar 31;22(1):184–98. https://doi.org/10.35784/acs_8247
53. Szabelski J, Karpiński R, Machrowska A. Application of an artificial neural network in the modelling of heat curing effects on the strength of adhesive joints at elevated temperature with imprecise adhesive mix ratios. Materials. 2022 Jan 18;15(3):721. https://doi.org/10.3390/ma15030721
54. Serani A, Scholcz TP, Vanzi V. A scoping review on simulation-based design optimization in marine engineering: Trends, best practices, and gaps. Arch Computat Methods Eng. 2024 Dec;31(8):4709–37. https://doi.org/10.1007/s11831-024-10127-1

55. Frazzica A, Manzan M, Palomba V, Brancato V, Freni A, Pezzi A, et al. Experimental validation and numerical simulation of a hybrid sensible-latent thermal energy storage for hot water provision on ships. Energies. 2022 Apr 2;15(7):2596. https://doi.org/10.3390/en15072596
56. Huner U, Irsel G, Bekar U, Szala M. A comprehensive case study to the implicit and explicit approach in finite element analysis. Adv Sci Technol Res J. 2024 Dec 7;19(2):407–17. https://doi.org/10.12913/22998624/196987
57. Hou Z, Yuan R, Chen Y, Sun W. Crack propagation process in double-flawed granite under compression using digital image correlation method and numerical simulation. Sci Rep. 2024 Sep 13;14(1):21424. https://doi.org/10.1038/s41598-024-72302-5
58. Li Y, Hu Y, Zheng H. Influence of bedding on fracture toughness and failure patterns of anisotropic shale. Engineering Geology. 2024 Nov;341:107730. https://doi.org/10.1016/j.enggeo.2024.107730
59. Chen X, Yu H, Zhong Y, Wang Q, Wu H. 3D XFEM for fluid-driven fracturing of layered anisotropic rock. Computer Methods in Applied Mechanics and Engineering. 2025 Jun;441:117963. doi:10.1016/j.cma.2025.117963
60. Zhou C, Lang Z, Huang S, Dong Q, Wang Y, Zheng W. A comprehensive review of experimental studies on shear behavior of bolted rock joints with varying rock joint and bolt parameters and normal stress. Deep Underground Science and Engineering. 2025 Jun;4(2):189–209. https://doi.org/10.1002/dug2.12091